

Monitoring copper ions in C. elegans using porphyrin phosphonic acids

Patrik Tholen, Ann-Kathrin Weishaupt, Franz-Josef Schmitt, Tim Müller, Jonas Fabrizi, Tuong V. M. Nguyen, Claudia Keil, Maria Maares, Lutz Schomburg, Hajo Haase, Yunus Zorlu, Jens Beckmann, Julia Bornhorst & Gündog Yücesan

Article - Version of Record

# Suggested Citation:

Tholen, P., Weishaupt, A.-K., Schmitt, F.-J., Müller, T., Fabrizi, J., Nguyen, T. V. M., Keil, C., Maares, M., Schomburg, L., Haase, H., Zorlu, Y., Beckmann, J., Bornhorst, J., & Yücesan, G. (2025). Monitoring copper ions in C. elegans using porphyrin phosphonic acids. Communications Materials, 6, Article 228. https://doi.org/10.1038/s43246-025-00975-0

# Wissen, wo das Wissen ist.



This version is available at:

URN: https://nbn-resolving.org/urn:nbn:de:hbz:061-20251111-123304-3

Terms of Use:

This work is licensed under the Creative Commons Attribution 4.0 International License.

For more information see: https://creativecommons.org/licenses/by/4.0

A Nature Portfolio journal



https://doi.org/10.1038/s43246-025-00975-0

# Monitoring copper ions in *C. elegans* using porphyrin phosphonic acids

Check for updates

Patrik Tholen¹, Ann-Kathrin Weishaupt², Franz-Josef Schmitt³, Tim Müller⁴, Jonas Fabrizi⁴, Tuong V. M. Nguyen¹, Claudia Keil 📵¹ ⊠, Maria Maares 📵⁵, Lutz Schomburg 📵⁶, Hajo Haase 📵¹, Yunus Zorlu 📵ˀ, Jens Beckmann 📵ී, Julia Bornhorst² & Gündog Yücesan 📵⁴ ⊠

Herein we report a charge-assisted hydrogen bonded organic framework (HOF) built with an extended tethered phosphonic acid namely 5,10,15,20-Tetra-(4'-yl-[1',1"-biphenyl]—4"phosphonic acid) porphyrin (p-H<sub>8</sub>-TBPPA) and phenyl phosphonic acid (PPA). Metal responsive fluorescent properties of the linker p-H<sub>8</sub>-TBPPA with biologically significant transition metal ions (Zn<sup>2+</sup>, Cu<sup>2+</sup>, Ni<sup>2+</sup>, Co<sup>2+</sup>, Fe<sup>2+</sup>, Mn<sup>2+</sup>) and heavy metal ions (Hg<sup>2+</sup>, Pb<sup>2+</sup>, Cd<sup>2+</sup>) is further characterized. p-H<sub>8</sub>-TBPPA shows distinct fluorescence responses for each metal ion with very specific decreases in intensity for the different analytes, and the strong turn off fluorescence of p-H<sub>8</sub>-TBPPA in presence of copper is used to monitor copper ion homeostasis in C. elegans. p-H<sub>8</sub>-TBPPA is also found to be non-toxic for Caco-2 cells and C. elegans at concentrations required for fluorescence measurements. These findings establish p-H<sub>8</sub>-TBPPA as a promising platform for the development of in vivo metal ion sensors, with potential applications in diagnostic imaging, and environmental monitoring.

Copper homeostasis in mammals requires complex regulation of absorption, storage, utilization, and excretion to prevent adverse consequences across a relatively broad spectrum of dietary exposure<sup>1</sup>. Defects in the pathways that regulate copper homeostasis can have serious health consequences, particularly for brain health and development, making them a risk factor for Alzheimer's and Parkinson's diseases2. Although copper homeostasis is tightly regulated, the underlying mechanisms of this regulation remain unclear and require further investigation through in vivo studies. Advances in non-invasive imaging techniques, particularly those using fluorescent probes for dynamic mapping of essential metals, present a valuable opportunity to analyze the localization and dynamics of labile copper (often referred to as loosely bound copper in the literature) in living organisms<sup>3-5</sup>, such as the model nematode Caenorhabditis elegans (C. elegans), by estimating probe signal intensities in fluorescence readouts. However, the application of copper-responsive fluorescent probes in C. elegans remains limited in the literature. While only a few ratiometric Cu(II) sensors with traditional chelating functional groups based on organic fluorophores such as naphthalimide and rhodamine have been reported to monitor cellular Cu(II)6, the use of high-affinity, non-chelating phosphonate groups directly appended to aromatic fluorophores is an emerging strategy for metal ion sensing, offering opportunities for biological applications  $\bar{\ }$  .

Therefore, we applied our recent design strategy on copper binding to fluorescent porphyrin phosphonic acids to develop cell-tolerable imaging agents suitable for in vivo copper imaging. We used C. elegans as a model organism to monitor copper homeostasis using p-H<sub>8</sub>-TBPPA ((5,10,15,20-Tetra-(4'-yl-[1',1"-biphenyl]-4"phosphonic acid)porphyrin)) and p-H<sub>8</sub>-TPPA with a porphyrin core, which exhibit high copper selectivity and show fluorescence quenching upon copper binding8. The number of metal ion responsive and selective fluorescent probes in the literature, especially for copper ions, are very limited<sup>9</sup>. Terminal polar phosphonic acid groups have a high metal binding affinity and selectivity for copper ions. This can be coupled with porphyrin and other fluorescent cores to generate metal responsive fluorescent probes with high affinity metal binding 10,11. The early work on phosphonate chelators by Martell had shown that phosphonate analogue ethylenediamine-N,N,N',N'-tetrakis(methylenephosphonic) acid of EDTA, generated 4.5 magnitudes of order stronger copper binding compared to EDTA, which is also higher compared to the currently studied other transition metal ions<sup>12</sup>. Therefore, in this work, we wanted to build up on our previous results with porphyrin-based sensors and generated a

¹Technische Universität Berlin, Chair of Food Chemistry and Toxicology, Berlin, Germany. ²Food Chemistry With Focus On Toxicology, Faculty of Mathematics and Natural Sciences, University of Wuppertal, Wuppertal, Germany. ³Institute of Physics, Martin Luther University Halle-Wittenberg, Halle (Saale), Germany. ⁴Institute for Inorganic Chemistry and Structural Chemistry, Heinrich Heine University Düsseldorf, Düsseldorf, Germany. ⁵Department of Food Chemistry, Institute of Nutritional Science, University of Potsdam, Nuthetal, Germany. ⁵Institut für Experimentelle Endokrinologie, Campus Charité Mitte, Berlin, Germany. ⁻Department of Chemistry, Gebze Technical University, Kocaeli, Istanbul, Turkey. ⁵Institut für Anorganische Chemie und Kristallographie, Universität Bremen, Bremen, Germany. ⊠e-mail: c.keil@tu-berlin.de; quendog,vuecesan@hhu.de

longer tethered version of the linker  $(p\text{-H}_8\text{-TBPPA})$  to monitor copper ions along with the shorter tethered version  $(p\text{-H}_8\text{-TPPA})^{7.8}$ . Copper is the third most abundant trace element with about 50--100 mg of total amount in the human body<sup>13</sup>. It is present in all tissues of the body, especially within the liver, brain, heart, kidneys and muscles<sup>14</sup>. Copper is an essential micronutrient involved in several vital processes, especially due to its capability to participate in redox reactions, but the redox capability of copper may also be deleterious to cell membranes, DNA and proteins when the metal is accumulated in excess<sup>2,14</sup>. In this work we report that metal responsive fluorophores like  $p\text{-H}_8\text{-TBPPA}$  and  $p\text{-H}_8\text{-TPPA}$  are useful for monitoring metal ions in biological systems, as metal ion homeostasis including copper homeostasis remains to be one of the least understood research areas<sup>7,8</sup>.

Metal binding fluorophores with phosphonic acid functional groups can crystallize as hydrogen bonded organic framework forms (HOFs)<sup>15,16</sup>. Single crystal structure determination of p-H<sub>8</sub>-TBPPA indicated the formation of a HOF structure as seen in Fig. 1. HOFs has been recently emerging as a rising class of microporous materials many applications of HOFs have been reported in drug delivery, small molecule storage, proton conductivity, optoelectronics and electrical conductivity 15-18. HOFs can be constructed using non-toxic organic compounds, and HOFs constructed using such organic compounds are useful especially for biological applications where slow dissociating microporous platforms for drug delivery and sensing are needed<sup>19-21</sup>. HOFs have been recently shown to be effective drug delivery agents and successfully used in chemical sensing<sup>21,22</sup>. Another advantage of HOFs over MOFs and COFs is that dissociated linker molecules from HOF crystals can be recrystallized and used sustainably, and HOFs usually provide greener synthesis routes compared to MOFs and COFs<sup>23</sup>. Among other HOF families, phosphonic acid HOFs stand out with respect to their excellent stability in humidity, proton conductivity and their sustainable transformation into covalent organic frameworks at temperatures above 210 °C<sup>16,17,23-26</sup>. Phosphonic acid is one of the least explored functional groups used in HOF synthesis<sup>24</sup>. Therefore, in addition to copper sensing, in this work, we report textural properties of the single crystal structure of of p-H<sub>8</sub>-TBPPA crystallizing as a phosphonic acid HOF (derived from p-H<sub>8</sub>-TBPPA and phenyl phosphonic acid). Furthermore, we report the crystal structure of its ester precursor of p-H<sub>8</sub>-TBPPA (5,10,15,20-Tetra-(1'-yl-[4',4"-biphenyl]-1"-dimethylphosphono)porphyrin), which we call p-Me<sub>8</sub>-TBPPE (See Fig. 1 and Fig. 2).

# Results and Discussion Synthesis

We report a synthesis route for biphenylphosphonate-functionalized porphyrin p-H<sub>8</sub>-TBPPA (5,10,15,20-tetra-(4'-yl-[1',1"-biphenyl]-4"phosphonic acid)porphyrin) and its precursor p-Me<sub>8</sub>-TBPPE (5,10,15,20-tetra-(1'-yl-[4',4"-biphenyl]—1"-dimethylphosphono)porphyrin) using a slightly modified Pd catalyzed Suzuki Coupling with p-Br<sub>4</sub>-TPP (5,10,15,20-tetra-(p-bromophenyl)porphyrin) and 4-dimethylphosphonophenyl boronic acid in the presence of [Pd(PPh<sub>3</sub>)<sub>4</sub>]<sup>27</sup>. p-Br<sub>4</sub>-TPP was synthesized according the literature<sup>28</sup> using 4-bromobenzaldehyde and pyrrole. 4-Dimethylphosphonophenyl boronic acid was synthesized from 1,4dibromobenzene, trimethyl borate and trimethyl phosphite according to literature<sup>27</sup>. The resulting p-Me<sub>8</sub>-TBPPE was then hydrolyzed in 37% HCl at 90 °C for 24 h to yield the final phosphonic acid p-H<sub>8</sub>-TBPPA (see Supplementary Fig. S1 and Supplementary Fig. S2 for the synthetic routes and Supplementary Fig. S3 and Supplementary Fig. S4 for the <sup>1</sup>H-NMR and <sup>31</sup>P-NMR spectra). A different synthetic approach for the synthesis of p-H<sub>8</sub>-TBPPA and its ethyl ester form p-Et<sub>8</sub>-TBPPE was reported by Bujoli in  $1998^{29}$ .

Synthesis of HOF p-H<sub>8</sub>-TBPPA-PPA. The single crystals of HOF were obtained following a similar route as for our previously reported phosphonic acid HOF GTUB5<sup>15,16</sup>. 5,10,15,20-Tetra-(4'-yl-[1',1"-biphenyl]—4"phosphonic acid)porphyrin (5.0 mg, 4.04 µmol, 1 eq), phenylphoshonic acid (PPA) (95.7 mg, 605.3 µmol, 150 eq), DMF (0.8 mL) and MeOH (0.2 mL) are combined and sonicated until dissolved in a 5 mL glass vial with screw cap and aluminium liner. A sealed glass vial is placed in an oven at 80 °C for 72 h. Dark purple needle shaped crystals of p-H<sub>8</sub>-TBPPA-PPA that are suitable for single crystal X-ray diffraction were collected after storing the glass vial at room temperature for 24 h.

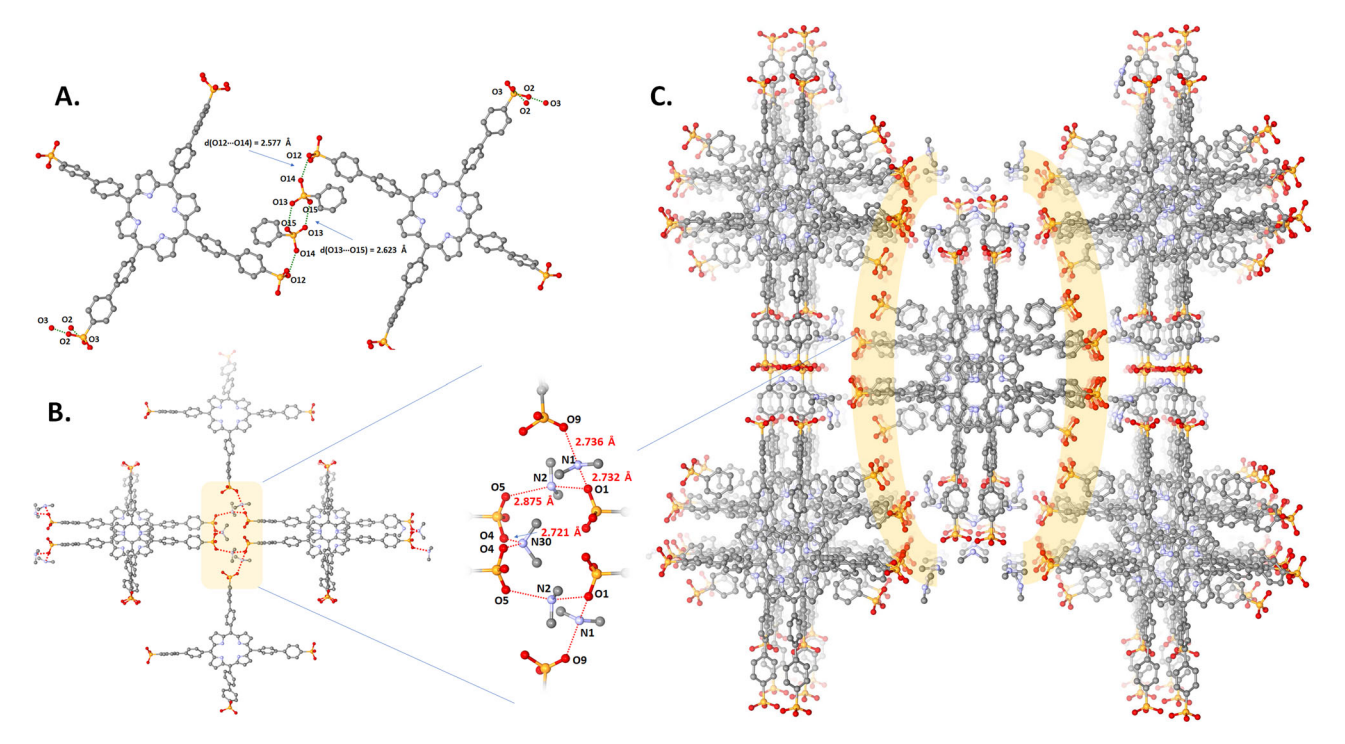
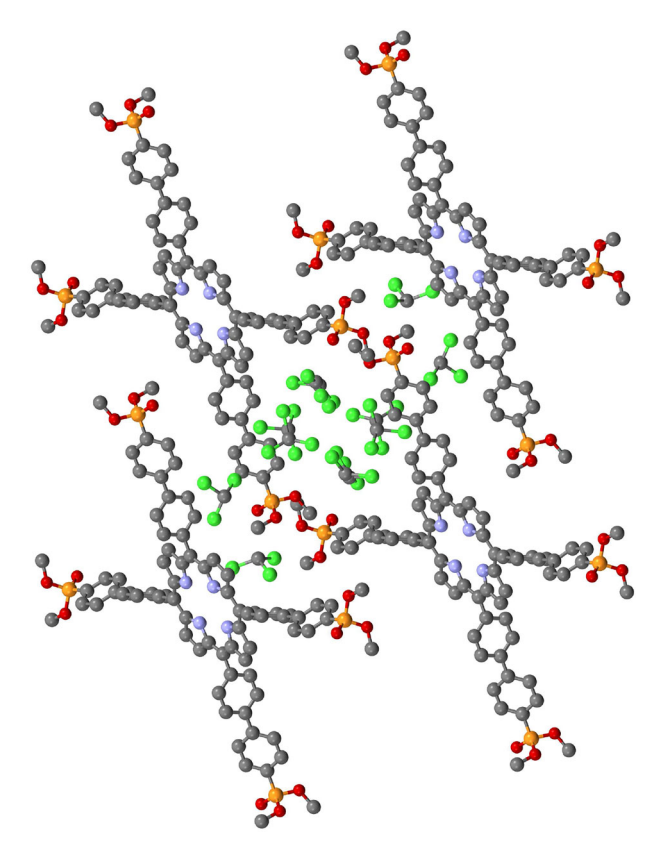


Fig. 1 | Crystal structure and hydrogen bonding interactions of p-H<sub>8</sub>-TBPPA-PPA. A The crystal structure of p-H<sub>8</sub>-TBPPA-PPA with hydrogen bonding pattern between the phosphonic acid functional groups. B The HOF structure with square

pores, which is constructed using the linker p-H<sub>8</sub>-TBPPA. C Hydrogen bonding pattern between the phosphonate groups of p-H<sub>8</sub>-TBPPA, PPA, and DMA $^+$  cations.



**Fig. 2** | **Solvent-filled crystal structure of** *p***-Me**<sub>8</sub>**-TBPPE.** Crystal structure of *p*-Me<sub>8</sub>**-TBPPE** with solvent molecules chloroform occupying the void channels.

**Crystallization of the** *p***-Me**<sub>8</sub>**-TBPPE**. Dark green powder of *p*-Me<sub>8</sub>-TBPPE was completely dissolved in chloroform to make a highly saturated solution. Suitable purple block-shaped crystals for X-ray analysis appeared after slow evaporation of chloroform at room temperature.

Crystal structure description of HOF p-H<sub>8</sub>-TBPPA-PPA and its ester form *p*-Me<sub>8</sub>-TBPPE. As seen in Fig. 1A, HOF *p*-H<sub>8</sub>-TBPPA-PPA creates very complex charge-assisted hydrogen bonded building units with DMA<sup>+</sup> cations and deprotonated phosphonic acid moieties. The shorter donor-acceptor oxygen distances below 2.4 Å are thought to have near covalent bond strength<sup>30</sup>. The donor-acceptor oxygen distances in HOF p-H<sub>8</sub>-TBPPA-PPA are observed to be 2.577 Å for d(O12-O14) and 2.623 Å for d(O13-O15). As seen in Fig. 1B the donor acceptor distances between the DMA<sup>+</sup> nitrogen atoms and phosphonic acid oxygen atoms provide a more complex pattern with a range between 2.721 Å and 2.875 Å. As seen in Fig. 1C, the crystal structure of p-H<sub>8</sub>-TBPPA-PPA indicates a compact alignment of X shaped p-H<sub>8</sub>-TBPPA linker generating large square shaped void channels, which are filled by deprotonated phenylphosphonic acids and DMA<sup>+</sup> cations. Due to the presence of long phenyl arms, the X shaped p-Me<sub>8</sub>-TBPPE, its crystal structure forms large voids filled by the solvent chloroform molecules. As seen in Fig. 2, the presence of methyl groups in the ester form blocked the formation of stronger van der Waals interactions between the p-Me<sub>8</sub>-TBPPE moieties. Despite its high theoretically simulated surface area, the ester form p-Me<sub>8</sub>-TBPPE is not expected to be permanently microporous due to the presence of relatively weaker van der Waals interactions holding the crystal structure together.

Surface area characterization of p-H<sub>8</sub>-TBPPA-PPA and its ester form p-Me<sub>8</sub>-TBPPE. There is one other report about the organic synthesis of p-H<sub>8</sub>-TBPPA and its ethyl ester p-Et<sub>8</sub>-TBPPE in the literature from 1998 without a crystal structure, where the non-crystalline linker

was found to be permanently microporous with a surface area of 470 m²/g after activation at  $180 \,^{\circ}\text{C}^{29}$ . As we report the first-time synthesis and crystal structure of a HOF constructed with  $p\text{-H}_8\text{-TBPPA}$ , we explored the textural properties of HOF  $p\text{-H}_8\text{-TBPPA}$ -PPA and its previously not reported methyl ester form  $p\text{-Me}_8\text{-TBPPE}$  without removing the solvent molecules and DMA<sup>+</sup> cations. The N<sub>2</sub> accessible geometric surface areas and Helium accessible pore volumes of as synthesized (i.e., solvent filled)  $p\text{-Me}_8\text{-TBPPE}$  and  $p\text{-H}_8\text{-TBPPA}$ -PPA were calculated using the Pore-Blazer v4 software <sup>31–33</sup>. While the pores of  $p\text{-H}_8\text{-TBPPA}$ -PPA was found to be inaccessible to N<sub>2</sub> without removing the solvent molecules, N<sub>2</sub> accessible geometric surface area and Helium accessible pore volume of  $p\text{-Me}_8\text{-TBPPE}$  were calculated as  $488 \, \text{m}^2/\text{g}$  and  $0.39 \, \text{cm}^3/\text{g}$ , respectively.

#### Absorbance and fluorescence properties of p-H<sub>8</sub>-TBPPA

First, the general absorbance (Fig. 3) and the fluorescence emission spectra (Fig. 4) of pure p-H<sub>8</sub>-TBPPA (1) and after addition of metal-ions were measured. Figure 3A shows the typical Soret peak at 415 nm as strongest absorption of the transition from the ground state to the second excited state (S0 → S2). Furthermore, a second region, the so-called Q-bands, were observed with wavelengths of 524 nm, 562 nm, 594 nm, and 652 nm (see Fig. 3D-F). According to M. Gouterman's four-orbital model, these Q-bands result from transitions from the ground state to the first excited state (S0  $\rightarrow$  S1) while the HOMO was calculated to be a  $a1_{\rm u}$  and  $a2_{\rm u}$  orbital and the LUMO consists of a degenerate set of  $e_{\rm g}$  orbitals  $^{34}\!.$  These Q-bands are characteristic for porphyrin molecules  $^{35-37}$ . The spectra of p-H<sub>8</sub>-TBPPA treated with either Co<sup>2+</sup>, Zn<sup>2+</sup>or Ni<sup>2+</sup> show a moderate hypochromic effect in both, the Soret peak and the Q-bands (Fig. 3A). A bigger difference can be observed in the presence of Pb<sup>2+</sup>, Cd<sup>2+</sup> and Mn<sup>2+</sup> (Fig. 3B). In addition to a small hypochromic effect, a hypochromic effect on the Soret peak and a bathochromic effect on the Q-bands can be observed. The soret peak shifts from 415 nm to 410 nm respectively and the Q-bands shift to 526 nm (524 nm), 566 nm (562 nm), 596 nm (594 nm) and 656 nm (652 nm). The biggest effect can be seen following the addition of Cu<sup>2+</sup>, Fe<sup>2+</sup>, and Hg<sup>2+</sup>. For Cu<sup>2+</sup> (Fig. 3C), the Soret peak shifts even stronger to shorter wavelengths (415 nm to 408 nm) and the first and second Q-bands merge into one, indicating stronger interaction of the metal to the porphyrin center. Iron treatment leads to a much higher absorbance (hyperchromic effect) for all observed peaks (soret peak and Q-bands) as compared to all other tested metals. Mercury on the other hand causes a shift and a split of the soret band to higher wavelengths (415 nm to 448 nm). The Q-bands merge at 640 nm. In addition to that, the whole spectra lose intensity in a hypochromic effect.

In Fig. 4A, the fluorescence emission scans are depicted with a typical maximum at 665 nm for the p-H<sub>8</sub>-TBPPA, when excited with 415 nm in the maximum of the absorbance. Furthermore, a typical second local maximum can be found at 710 nm. These dual emission peaks are characteristic for porphyrins in general and result from the (S1  $\rightarrow$  S0) relaxation in the long wavelength Q-bands<sup>38-40</sup>. A 3D-plot of the excitation-emission scan is provided in the supporting information (Supplementary Fig. S5) to point out the characteristics of p-H<sub>8</sub>-TBPPA in a buffer solution at physiological pH. Ni<sup>2+</sup> and Fe<sup>2+</sup> ions do not alter the fluorescence emission of the p-H<sub>8</sub>-TBPPA sensor (Fig. 4A). Certain quenching effects can be seen following addition of  $Hg^{2+}$  and  $Mn^{2+}$  (Fig. 4B). While the two characteristic emission peaks are still observable, the overall intensity drops to nearly 50% of the untreated p-H<sub>8</sub>-TBPPA when treated with Mn<sup>2+</sup> ions. The strongest effects can be seen for Cu<sup>2+</sup>, Pb<sup>2+</sup>, Cd<sup>2+</sup>, Co<sup>2+</sup>, and Zn<sup>2+</sup> (Fig. 4C) where the intensities decrease immensely. All these data indicate that p-H<sub>8</sub>-TBPPA is a highly dynamic fluorescent probe that provides a unique response to the presence of different metal ions, offering potential for further development as a platform for sensing multiple metal ions.

#### Fluorescence lifetime

As a good tool to solve interaction mechanisms between fluorescent probes and their surroundings, including specific metal-ions, time-resolved fluorescence spectroscopy proved to be highly efficient<sup>41,42</sup>. The quantitative study of dynamic electronic interactions between metal ions and the

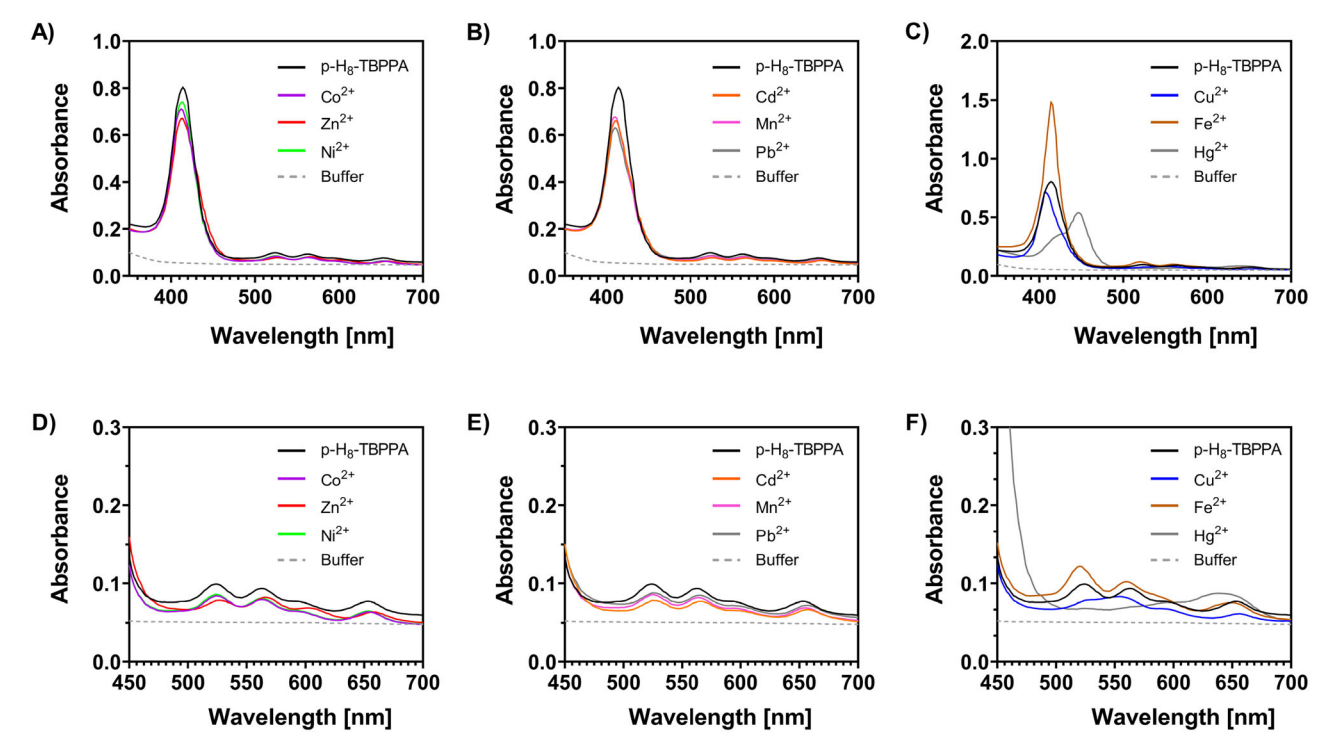
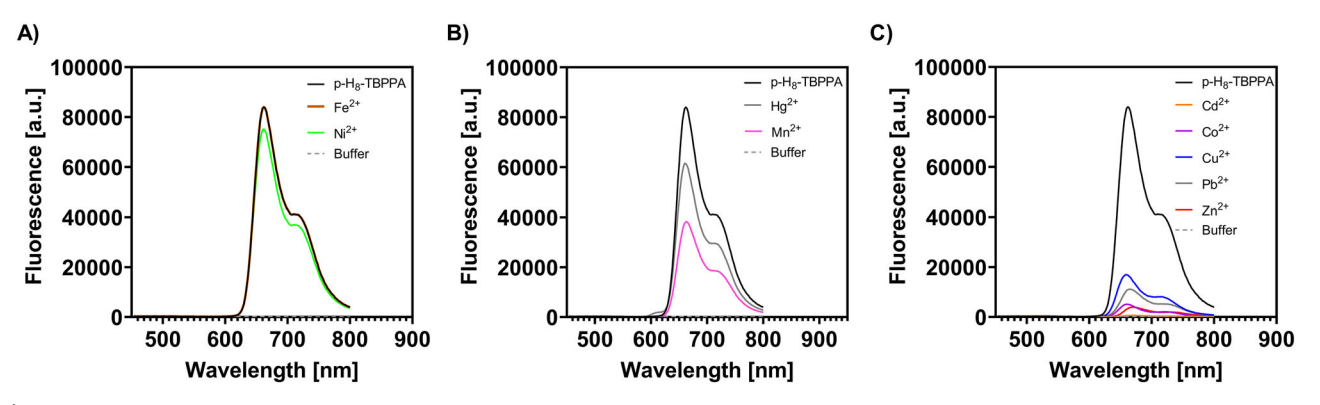


Fig. 3 | Absorbance response of p-H<sub>8</sub>-TBPPA to metal ions. Metal-dependent changes in p-H<sub>8</sub>-TBPPA (final concentration 10  $\mu$ M) absorbance properties treated with either 50 mM HEPES buffer or with buffer containing various metal solutions

(final concentration 40  $\mu M).$  From left to right: A/D  $Co^{2+},$   $Zn^{2+},$   $Ni^{2+};$  B/E  $Cd^{2+},$   $Mn^{2+},$  Pb $^{2+};$  C/F  $Cu^{2+},$  Fe $^{2+},$  Hg $^{2+}.$ 



**Fig. 4** | **Metal-dependent fluorescence changes of** p-H<sub>8</sub>-TBPPA. Metal-dependent changes in p-H<sub>8</sub>-TBPPA (final concentration 10  $\mu$ M) fluorescence emission properties ( $\lambda_{\rm ex}$  = 415 nm) treated with either 50 mM HEPES buffer or with HEPES buffer

containing various metal solutions (final concentration 40  $\mu$ M) before recording; left to right: (A) Fe²+, Ni²+; (B) Hg²+, Mn²+; (C) Cd²+, Co²+, Cu²+, Pb²+, Zn²+. Data are representative for three independent experiments.

fluorescence showed characteristic changes in fluorescence intensity and lifetime<sup>43</sup>. Generally, structural molecular changes correlate with the measured fluorescence lifetime offering a tool to quantitatively understand different mechanisms of fluorescence quenching<sup>44–46</sup>.

In more detail, the time-resolved fluorescence showed a strong dose-dependency of the  $p\text{-H}_8\text{-TBPPA}$  fluorescence decay curves for Cu²+ at concentration between 0 and 30  $\mu\text{M}$  (See Fig. 5). The time-course of the fluorescence of the pure dye decays monoexponentially with 7.2 + /-0.1 ns while after addition of 10 and 20  $\mu\text{M}$  CuSO4 three exponential functions are necessary to obtain a sufficient fit. The time constants are 320+/-50 ps, 1.4+/-0.1 ns and 6.9+/-0.1 ns for  $10~\mu\text{M}$  CuSO4 and 170+/-50 ps, 0.7+/-0.1 ns and 3.7+/-0.1 ns for  $20~\mu\text{M}$  CuSO4 with strongly reduced amplitudes of the long components. At  $30~\mu\text{M}$  CuSO4 a single exponential decay with 160+/-50 ps time constant was obtained.

At lower copper concentrations, the quenching is mainly dynamic as the fluorescence lifetime changes with increasing

concentration of the quencher. The copper quenching becomes static at higher concentrations leading to a lifetime change and amplitude drop of the fluorescence (see Figs. 4, 5) indicating that stable complexes might be formed between  $p\text{-H}_8\text{-TBPPA}$  and copper ions possibly due to a molecular change (e.g., oxidation of the molecule). Our previous publication of photoluminescence decay curves of GTUB-5-Cu crystals, where Cu(II) ions were inserted specifically into porphyrin core resulted in relatively long photoluminescence lifetimes<sup>47</sup>. The shortened fluorescence decay time for  $p\text{-H}_8\text{-TBPPA}$  might be indicative that predominantly the  $p\text{-H}_8\text{-TBPPA}$  phosphonic acid groups are coordinating to Cu(II) ions.

#### Ceruloplasmin

Serum Cu<sup>2+</sup> species are being explored as potential diagnostic indicators for monitoring changes in copper homeostasis linked to disease progression<sup>3</sup>. With the further aim of using the sensor for fluorimetric copper detection in biofluids, in particular for the determination of copper in serum samples, we

carried out a series of experiments to unravel interaction of  $p\text{-H}_8\text{-TBPPA}$  with copper incorporated into ceruloplasmin - the major copper-containing protein in mammalian serum. To do so, first a Cu-titration was carried out, intending to value the half maximal effective concentration (EC $_{50}$ ) of copper for  $p\text{-H}_8\text{-TBPPA}$  fluorescence quenching upon 0–20  $\mu\text{M}$  CuSO $_4$  treatment. After transformation, normalizing, and nonlinear fitting of the fluorescence dataset an EC $_{50}$  of 1.28  $\pm$  0.07  $\mu\text{M}$  was established (Fig. 6A), close to the EC $_{50}$  value reported for H $_8\text{-TPPA}^8$ .

Next, purified human holo-Ceruloplasmin containing six Cu $^{2+}$  ions per ceruloplasmin molecule (total copper concentration of the CP solution 219.92  $\pm$  6.59  $\mu M)$  (Chillon et al. $^{48}$ ) was compared to the fluorescence quenching efficacy of 1.25  $\mu M$  ( $\sim$  50% drop in  $H_8$ -TBPPA fluorescence) and 7.5  $\mu M$  CuSO $_4$  (less than 7.5% fluorescence remaining) (Fig. 6B) $^{48}$ . The 3D scans show that Cu-Holo-CP hardly shows any self-fluorescence in the range of the parameters of p-H $_8$ -TBPPA (Supplementary Fig. S6). At 7.5  $\mu M$  copper provided as Cu-Ceruloplasmin a reduction of p-H $_8$ -TBPPA fluorescence by about 50% was observed, indicating a one Cu $^{2+}$ -equivalent detection either released from CP (labile copper) or copper accessible for the sensor though still incorporated into the protein core. Our previous

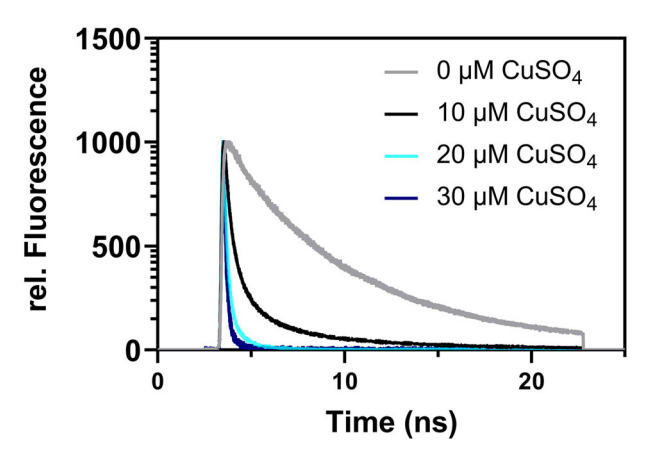


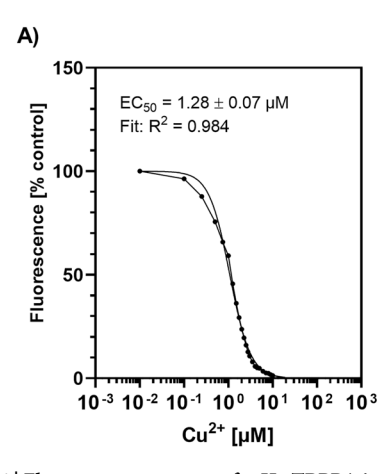
Fig. 5 | Fluorescence decay curves of p-H<sub>8</sub>-TBPPA at 665 nm in the presence of CuSO<sub>4</sub>. Time-resolved fluorescence was excited with 405 nm on solution of  $10~\mu M$  p-H<sub>8</sub>-TBPPA in the presence of various concentrations of CuSO<sub>4</sub> between 0 and  $30~\mu M$ . Shown are relative signal intensities normalized to 1000 for all concentrations.

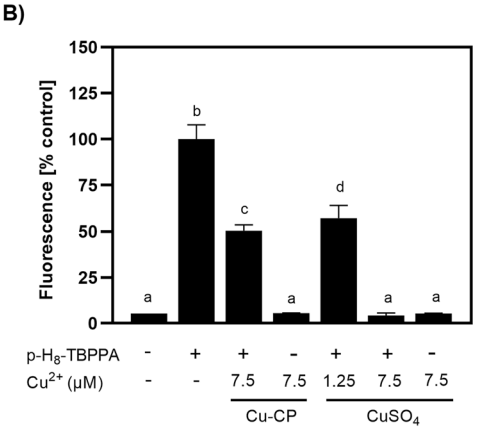
investigations led to conclusion of almost irreversible molecule change when treating p-H<sub>8</sub>-TPPA with CuSO<sub>4</sub> as this interaction could not be reversed even by the addition of strong metal complexing agents<sup>8</sup>. In this study for the extended p-H<sub>8</sub>-TBPPA bisphenylphosphonate-tethered porphyrin however, post-treatment with EDTA led to significant reversal effects in the case of CuSO<sub>4</sub>; a first indication that the expansion of the porphyrin phosphonate side chain has a significant effect on the modality of the sensor-copper interaction. The Cu-Ceruloplasmin- exposed sensor on the other hand remained quenched even after addition of EDTA. Literature indicates that metallized CP remains stable in its copper centers, even when exposed to high EDTA concentrations<sup>8,49</sup>. The perpetuation of the Cu-CP mediated p-H<sub>8</sub>-TBPPA quenching even after a reasonable EDTA treatment could be rated as an indication that the sensor is able to enter into ternary complexes with copper-occupied ceruloplasmin.

#### Cytotoxicity

Cytotoxicity was studied by testing the cell viability of differentiated human intestinal Caco-2 cells following long term incubation (24 h) with different amounts of p-H<sub>8</sub>-TBPPA by analysing cell metabolic activity. Increasing concentrations of p-H<sub>8</sub>-TBPPA had no statistically significant effect on cell viability to up to  $202\,\mu\text{M}$  when compared to media control treatment (Fig. 7A). Along with cytocompatibility testing p-H<sub>8</sub>-TBPPA cell labelling efficiency was investigated. Figure 7B shows the Caco-2 cell fluorescence after 24 h incubation with nontoxic levels of p-H<sub>8</sub>-TBPPA. Increasing sensor concentration in the incubation medium led to higher cellular fluorescence with a saturation following 101 µM p-H<sub>8</sub>-TBPPA treatment. The confocal microscopic pictures of the cells treated with the highest p-H<sub>8</sub>-TBPPA concentration show most of the fluorescence signal emitted from larger sensor aggregations on the cellular surface of the Caco-2 cells (Fig. 7C). Intracellular p-H<sub>8</sub>-TBPPA fluorescence was barely detectable or attenuated by the intense glow of the extracellular aggregates. In a direct comparison the shorter p-H<sub>8</sub>-TPPA aryl-phosphonate porphyrin sensor was much more dispersed in the cell interior, leading to better efficiency in intracellular cell labelling8.

Subsequently, a time series of Caco-2 associated p-H<sub>8</sub>-TBPPA metal responsiveness was measured (Fig. 8). For Hg<sup>2+</sup> and Pb<sup>2+</sup> the fluorescence signals remained at the p-H<sub>8</sub>-TBPPA baseline over the entire measurement period. A slight quenching was achieved with Cd<sup>2+</sup>, Ni<sup>2+</sup> and Co<sup>2+</sup> and Mn<sup>2+</sup> as already seen in the fluorescence spectra of the sensor in the absence of cells (Fig. 4). Following Zn<sup>2+</sup> addition, Caco-2 p-H<sub>8</sub>-TBPPA, fluorescence gradually decreased. The most obvious turn-off effects were observed following





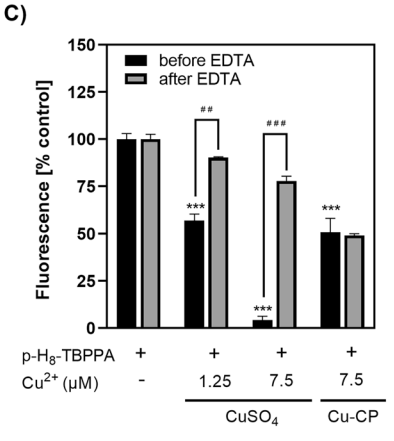
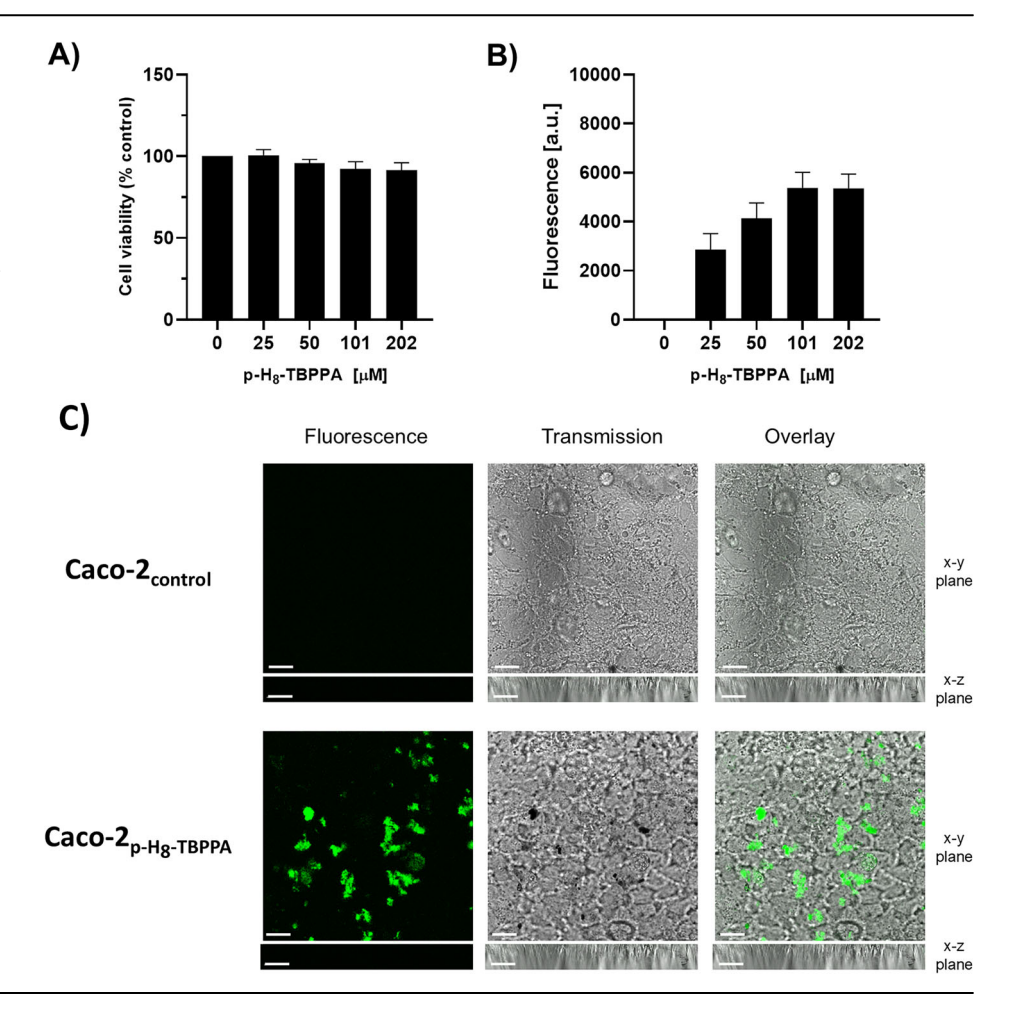


Fig. 6 | Fluorescence response of p-H $_8$ -TBPPA in the presence of CuSO $_4$  or Cu-Ceruloplasmin. A Fluorescence titration of p-H $_8$ -TBPPA (10  $\mu$ M solutions) by CuSO $_4$  (0–20  $\mu$ M). Sigmoidal dose-response curve was fitted by non-linear regression, and the resulting IC $_{50}$  value was indicated. B p-H $_8$ -TBPPA fluorescence after 30 min treatment with 1.25 or 7.5  $\mu$ M Cu $^{2+}$  from either CuSO $_4$  or Cu-Ceruloplasmin (Cu-CP). Bars sharing letters are not significantly different (repeated measures ANOVA with Tukey's multiple comparisons post-hoc test, p < 0.05). C Reversibility

of CuSO<sub>4</sub> or Cu-Ceruloplasmin induced H<sub>8</sub>-TBPPA quenching. Statistically significant differences from buffer incubation (\*\*\*p < 0.001; two-way ANOVA/ Tukey post hoc test) or from metal cation treatment (##p < 0.01; ###p < 0.001; two-way ANOVA/ Tukey post hoc test) are indicated. Fluorescence emission detection ( $\lambda_{\rm em} = 660$  nm,  $\lambda_{\rm ex} = 415$  nm). Data are means  $\pm$  SEM of n = 3 independent experiments.

Fig. 7 | Fluorescence labelling of Caco-2 enterocytes by p-H<sub>8</sub>-TBPPA. A MTT-Assay of differentiated human intestinal Caco-2 cells with p-H<sub>8</sub>-TBPPA concentrations of 25–202  $\mu$ M. B Fluorescence intensities of Caco-2 cells treated with 25–202  $\mu$ M p-H<sub>8</sub>-TBPPA ( $\lambda_{\rm em}$  = 660 nm,  $\lambda_{\rm ex}$  = 415 nm) (C) Confocal images of Caco-2 enterocytes in the presence or absence of p-H<sub>8</sub>-TBPPA (202  $\mu$ M solution). Scale bars: 10  $\mu$ m. Data are representative of n = 3 independent experiments.



 $\rm Fe^{2+}$  and  $\rm Cu^{2+}$  treatment. Caco-2  $p\text{-H}_8\text{-}TBPPA$  fluorescence drop in the presence of iron was contrary to the results obtained in cell-free measurements (Fig. 4). A plausible explanation could be that Caco-2's cellular homeostasis was overburdened by a supraphysiological amount of ferrous ions, causing Fenton-reaction oxidative stress and copper release detected by  $p\text{-H}_8\text{-}TBPPA^{50}$ .

#### Uptake in C. elegans

C. elegans has emerged as a highly amenable model to study trace element homeostasis, including iron, manganese and zinc<sup>43,51,52</sup>. Also, questions related to Cu homeostasis have been addressed but remained relatively unexploited compared to other trace elements<sup>4,53,54</sup>. To improve the power of using (bi)phenylphosphonate-functionalized porphyrins as copper probes in a living organism, fluorescence microscopy as well as a multi-well multi-worm analysis was performed. Results of both approaches were normalized to percentages of untreated control worms in order to identify changes upon Cu exposure and to compensate for interday variations, which commonly occur in living organisms. Optimal dye loading was achieved upon 3 h incubation with 50  $\mu$ M (bi)phenylphosphonate-functionalised porphyrins. Figure 9 shows regular distribution and reproducible intense signals in the p-H<sub>8</sub>-TBPPA or p-H<sub>8</sub>-TPPA treated control C. elegans microscopic pictures as well as the multi-well microplate measurements (Fig. 9).

#### **Conclusions**

Herein, we report the use of p-H<sub>8</sub>-TBPPA to monitor copper ions in C. *elegans* and further studied its metal responsiveness with a range of transition metal ions and heavy metal ions. We were able to obtain the crystal structure of the linker using the phenylphosphonic acid modulator that led a synthesis of a HOF structure with the crystal structure of a bi-linker

phosphonic acid HOF, namely p-H<sub>8</sub>-TBPPA-PPA, constructed using p-H<sub>8</sub>-TBPPA and PPA We also report the crystal structure of its methyl ester precursor. We further provide a synthetic pathway for the fabrication of p-H<sub>8</sub>-TBPPA linker. In order to test the suitability of p-H<sub>8</sub>-TBPPA for biological applications, we studied its toxicity and metal responsiveness in human intestinal Caco-2 cells. The viability of the cells was unaffected up to 202  $\mu$ M p-H<sub>8</sub>-TBPPA treatment and they responded to Zn<sup>2+</sup>, Fe<sup>2+</sup>, and even stronger to Cu<sup>2+</sup> by fluorescence quenching. Furthermore, we have used p-H<sub>8</sub>-TBPPA in C. elegans to monitor copper homeostasis in C. elegans and further studied its metal-responsive fluorescence properties. We have shown that p-H<sub>8</sub>-TBPPA is able to enter into ternary complexes with copper-occupied ceruloplasmin. The general knowledge in metal homeostasis in health and disease is still limited in the literature. There are very few tools available to monitor the roles of transition metal ions such as zinc and copper in the literature. Copper-responsive non-toxic fluorescent probes like p-H<sub>8</sub>-TBPPA for the studied cell lines can be developed to sense metal ions in biology. both arylphosphonate-tethered porphyrin Cu probes H<sub>8</sub>-TBPPA and its shorter form H<sub>8</sub>-TPPA are promising and exciting tools in order to identify potential alterations of available Cu in the nematode C. elegans. Compared to ICP-OES measurements, the usage of Cu(II)-specific probes is a less-time-consuming, cheap as well as a reliable non-destructive method allowing high throughput analysis of copper ions in a living organism. In addition to sensing copper ions, p-H<sub>8</sub>-TBPPA is a very dynamic sensing platform providing a unique fluorescent response to each of the studied metal ions. Furthermore, the development of phosphonic acid HOFs with non-toxic linker cores is important with respect to developing microporous materials targeting application in drug delivery, removal of toxins, and sensing applications.

Fig. 8 | Kinetics of Caco-2-associated p-H<sub>8</sub>-TBPPA metal responsiveness. Differentiated Caco-2 cells were loaded with 202  $\mu$ M p-H<sub>8</sub>-TBPPA for 24 h. A–C The fluorescence was recorded at 3 min intervals ( $\lambda_{\rm em}=660$  nm,  $\lambda_{\rm ex}=415$  nm). Fifteen minutes after the start of the experiment (5 cycles), metal salt solutions (final concentration 50  $\mu$ M) or buffer (control) were added and the fluorescence measurement was continued. D Summary of cellular p-H<sub>8</sub>-TBPPA responsiveness; data were taken from the last fluorescence readout shown in (A–C). Data are means  $\pm$  SEM of n=3 independent experiments.

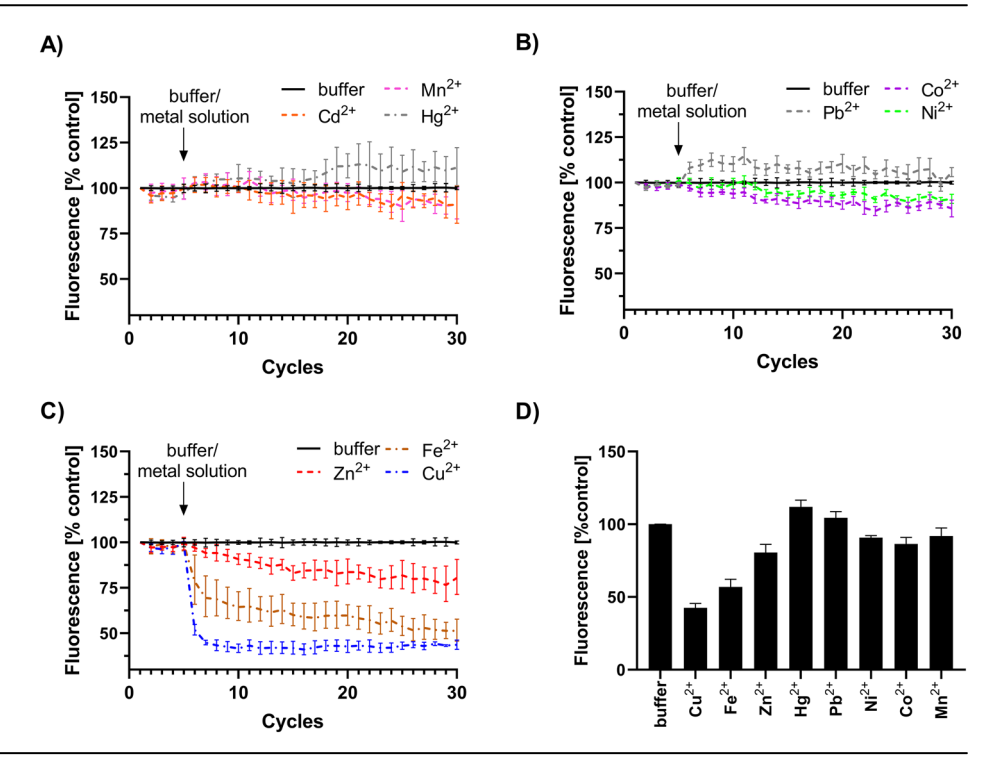
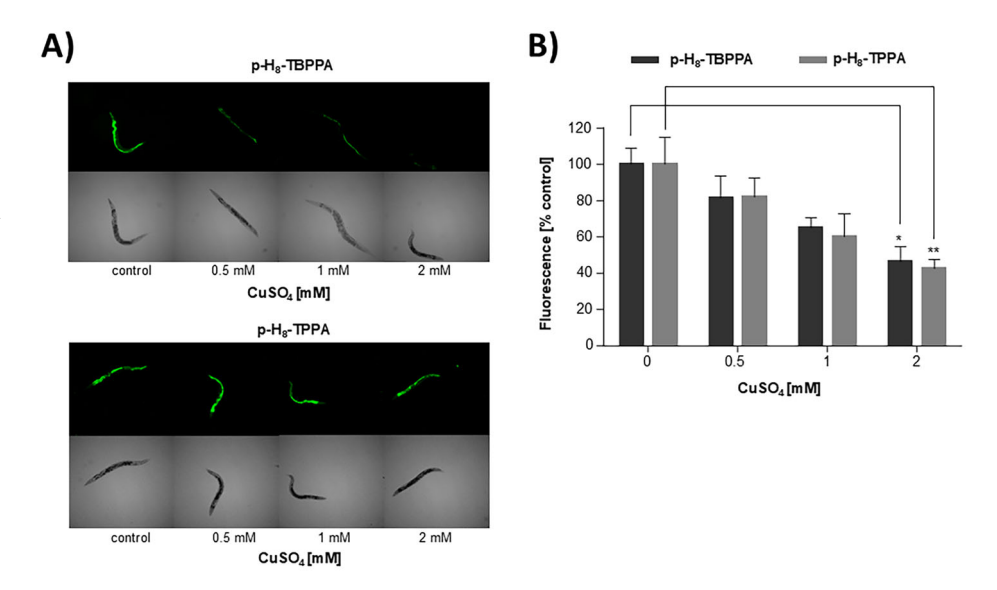


Fig. 9 | (Bi)phenylphosphonate-functionalized porphyrins as copper probes in *C. elegans*.

A Fluorescence and related bright field microscopic images as well as (B) microplate fluorescence measurements of living young adult *C. elegans* following 24 h copper exposure and postincubation with 50  $\mu$ M p-H<sub>8</sub>-TBPPA or p-H<sub>8</sub>-TPPA. Quantitative microplate data presented are mean values  $\pm$  SEM of n=4 independent experiments. The unpaired t-test was used for statistical analysis. \* $p \le 0.05$  and \*\* $p \le 0.01$  compared to untreated control. Cu exposure resulted in a reduced fluorescence of the (bi)phenylphosphonate-functionalised porphyrin probes compared to the untreated control worms. The results of the microscopy as well as multi-well approach are comparable.



#### Methods

# Synthesis of 5,10,15,20-Tetra-(1'-yl-[4',4"-biphenyl]-1"-dimethylphosphono)porphyrin

In a Suzuki-coupling reaction, 5,10,15,20-tetra-(4-bromophenyl)porphyrin (0.54 mmol, 500 mg), tetrakis-(triphenylphosphine)palladium (0.03 mmol, 31 mg), calciumcarbonate (5.37 mmol, 568 mg) and (4-(dimethoxyphsophoryl)phenyl)boronic acid (4.30 mmol, 988 mg) were dissolved in a mixture of toluene (50 mL), ethanol (25 mL) and water (25 mL) and refluxed for 24 h. Afterwards, the solvents were evaporated and the resulting precipitate was solved in chloroform ( $3 \times 50$  mL) and filtered. Afterwards, the filtrate was washed with 1 M HCl ( $3 \times 20$  mL), the organic layer dried over MgSO<sub>4</sub>, filtered, the solvents were evaporated and the precipitate dried under reduced pressure. The product results as dark green powder in good yields of 81 % (0.44 mmol, 599 mg). Suitable crystals for X-ray analysis were

grown from a saturated chloroform solution by slowly evaporating the solvent in the dark.

# Synthesis of 5,10,15,20-Tetra-(4'-yl-[1',1"-biphenyl]-4"phosphonic acid)porphyrin

In a round bottom flask equipped with magnetic stirring and condenser, 5,10,15,20-Tetra-(1'-yl-[4',4"-biphenyl]-1"-dimethylphosphono)porphyrin (0.370 mmol, 500 mg) was heated as emulsion in a HCl solution (36%, 20 mL) for 24 h at 80 °C. Afterwards, the precipitate was filtered off and washed several times with small amounts of water and dried under reduced pressure, yielding in a dark green powder (359  $\mu$ mol, 442 mg, 97%). Suitable crystals for X-ray analysis were grown by a the crystallisation method described below.

#### Crystallization of p-H<sub>8</sub>-TBPPA-PPA

In a 5 mL glass vial with screw cap and aluminium liner, 5,10,15,20-Tetra-(4'-yl-[1',1"-biphenyl]-4"phosphonic acid)porphyrin (5.0 mg, 4.04  $\mu$ mol, 1 eq), phenylphoshonic acid (95.7 mg, 605.3  $\mu$ mol, 150 eq), DMF (0.8 mL) and MeOH (0.2 mL) were combined and sonicated until dissolved. Afterwards, the cap was screwed tight, and the vial was placed in an oven at 80 °C for 72 h. Suitable crystals were received upon cooling and storing the vial in the dark at room temperature for 24 h.

# General measurements of absorption and fluorescence spectroscopy

Absorption spectra were recorded with a Tecan Infinite M200 Reader (Tecan Austria GmbH, Grödig/Salzburg, Switzerland) from 350 to 500 nm. The same device was used in fluorescence mode for fluorescence excitation  $(\lambda_{ex} 350-500 \text{ nm}; \lambda_{em} = 660 \text{ nm})$  and fluorescence emission scans  $(\lambda_{em} 550-$ 850 nm;  $\lambda_{ex} = 415$  nm) scans. 3D scanning was performed on a Spark® multimode microplate reader (Tecan Austria GmbH, Grödig/Salzburg, Switzerland) from 350 to 550 nm (Exc.) and 600 to 900 nm (Em.) with a 5 nm step size, excitation and emission bandwidths of 5 nm, and a detector gain of 100. A typical reaction mix was made by combining equal volumes of 20 μM phosphonate porphyrins diluted in assay-buffer (50 mM HEPES in bidistilled water adjusted to pH 6.5 with sodium hydroxide solution; depleted of multivalent cations with Chelex® 100 Resin pretreatment) and a double-concentrated metal cation solution<sup>55</sup>. Following 30 min incubations at 37 °C absorption or fluorescence measurements were done. p-H<sub>8</sub>-TBPPA response toward Holo-Ceruloplasmin was measured by treating 10 µM phosphonate porphyrins with 7.5 μM Cu<sup>2+</sup> provided as Cu-Ceruloplasmin (total copper concentration of the Cu-CP solution  $219.92 \pm 6.59 \,\mu\text{M}$ , six  $Cu^{2+}$  ions per ceruloplasmin) followed by either 3D scanning ( $\lambda_{ex}$  350-500 nm;  $\lambda_{em} = 600-900 \text{ nm}$ ) or fluorescence emission readout  $(\lambda_{\rm ex} = 415 \text{ nm}; \lambda_{\rm em} = 660 \text{ nm})^3$ . To evaluate the effect of metal chelators on CuSO<sub>4</sub> or Cu-Ceruloplasmin induced H<sub>8</sub>-TBPPA quenching measured by combining metal chelators, the metal cation-treated incubation mixtures were posttreated with 0.5 mM EDTA for 15 min before fluorescence emission readout.

### Fluorescence Lifetime

Time-Resolved Spectroscopy was performed in the single photon counting mode (TCSPC) using a setup analogous to that described in ref. 56. Measurements utilized a Hamamatsu R5900 16-channel multi-anode photomultiplier tube, featuring 16 distinct anode outputs and a shared cathode-dynode system (PML-16C, Becker&Hickl, Berlin, Germany). The spectrometer incorporated a 600 grooves/mm grating, achieving a spectral bandwidth of approximately 12.5 nm per channel allowing to determine the fluorescence decay at distinct wavelengths. Excitation was provided by a 405 nm pulsed laser diode (LDH-405, Picoquant, Berlin). Fluorescence decay was observed at room temperature in quartz suprasil cuvettes with a 3 mm path length (Thorlabs Inc., USA), facilitated by a 632 nm longpass filter (F76-631, AHF Analysentechnik, Tübingen, Germany). The excitation intensity was maintained at 80 W/m², with 300 seconds data accumulation time.

# Cell culture experiments

Caco-2 cells were obtained from the European Collection of Authenticated Cell Cultures (ECACC, Porton Down, UK). Cells were maintained in DMEM<sub>phenol red</sub> containing 10% fetal calf serum (FCS), 100 U/mL penicillin and 100 µg/mL streptomycin (PenStrep) at 37 °C in a humidified 5 % CO<sub>2</sub> atmosphere. For cellular phosphonate porphyrins experiments, cells were transferred into 96 well plates (initial seeding: 5000 cells per well) and cultured for 21 days for differentiation into an enterocyte-like monolayer. Subsequently, the cells were incubated with 0–202 µM p-H<sub>8</sub>-TBPPA diluted in DMEM<sub>white</sub>/PenStrep for 24 h<sup>57,58</sup>. Excess p-H<sub>8</sub>-TBPPA was removed by multiple washing steps before fluorescence emission detection (Tecan Infinite M200 Reader;  $\lambda_{ex} = 415$  nm;  $\lambda_{em} = 660$  nm). The metabolic activity of the cells was subsequently determined using the MTT assay<sup>59</sup>. 0.01% (v/v)

Triton X-100 was included as positiv control causing around 60% cytotoxicity. To analyze metal responsiveness of the Caco-2 associated phosphonate porphyrins (loading ON with 202  $\mu$ M p-H<sub>8</sub>-TBPPA), cells were post-treated with 50  $\mu$ M of different metal solutions at 37 °C in in a HEPES-based incubation buffer (10 mM HEPES, pH 7.35, 120 mM NaCl, 5.4 mM KCl, 5 mM glucose, 1.3 mM CaCl<sub>2</sub>, 1 mM MgCl<sub>2</sub>, 1 mM NaH<sub>2</sub>PO<sub>4</sub>) in a time-course experiment.

Fluorescence images of p-H<sub>8</sub>-TBPPA-labeled Caco-2 enterocytes were acquired on a Leica TCS SP8 laser scanning confocal microscope equipped with LAS X 3.5.5.19976 software platform, using a HC PL APO CS2 63x/1.20 water objective. The filters settings were  $\lambda_{ex}$  488 nm/  $\lambda_{em}$  580 nm; pinhole 111.5  $\mu m$ , pinhole size 1 AU $^{\rm S}$ .

Uptake in C. elegans: C. elegans strains and cultivation conditions:

*C. elegans* strain Bristol N2 (wildtype) was obtained from the Caenorhabditis Genetics Center (CGC), which is funded by the National Institutes of Health Office of Research Infrastructure Programs. The cultivation of *C. elegans* was performed on 8 P agar plates, coated with the *E. coli* strain NA22 at 20 °C as previously described in ref. 60. For each experiment adult worms were treated with bleach solution (1% NaOCl and 0.5 M NaOH) and eggs were isolated, before synchronous L1 stage larvae were placed on OP50 coated NGM agar plates for 48 hours to reach L4 stage.

# Copper exposure and phosphonate porphyrin loading

Synchronous L4 worms were treated with copper-enriched *E. coli* strain OP50 on agar plates for 24 h. Stock solutions of CuSO<sub>4</sub> (Sigma Aldrich, Germany, anhydrous powder,  $\geq$  99.99% purity) were prepared using sterile purified water (18 M $\Omega$ ) and diluted shortly before the experiment. The bacteria for feeding were inactivated to ensure the copper species (Cu<sup>2+</sup>) are not metabolized. *E. coli* strain OP50 inactivation was achieved by heat shocking (70 °C, 4 h). NGM agar plates were coated with 1 mL *E. coli* enriched with 0, 0.5, 1.0, and 2.0 mM CuSO<sub>4</sub>. 750 L4 worms were placed on each plate for 24 h till young adult stage.

After copper exposure, worms were removed from the agar plates by rinsing three times with incubation buffer (25 mM HEPES, 120 mM NaCl, 5.4 mM KCl, 5 mM Glucose, 1.3 mM CaCl<sub>2</sub>, 1 mM MgCl<sub>2</sub>, 1 mM NaH<sub>2</sub>PO<sub>4</sub>, pH = 7.35, 0.01% Tween). 1600 young adult worms per copper concentration were incubated in tubes with 50  $\mu$ M p-H<sub>8</sub>-TBPPA or p-H<sub>8</sub>-TPPA (stock solutions were diluted in DMSO), on a shaker in the dark for 3 h. After 90 min, tubes were ventilated to protect worms against oxygen deficiency. 4 washing steps were carried out to remove excess fluorescent dye.

# Fluorescence microscopy

Copper- and either p-H<sub>8</sub>-TBPPA or p-H<sub>8</sub>-TPPA -treated worms were transferred to 2% agarose pads on microscope slides and anesthetized with 5 mM levamisole (Sigma Aldrich, Germany). Fluorescence images were taken with a Leica DM6 B fluorescence microscope (Leica Microsystems GmbH) using a triple band excitation filter while preserving settings and light exposure times. Image processing was carried out by using the Leica LAS X software (Leica Microsystems GmbH).

## Loosely bound copper quantification via microplate reader

Tubes containing 1600 adult worms loaded with copper and posttreated with either  $p\text{-H}_8\text{-}TBPPA$  or  $p\text{-H}_8\text{-}TPPA$ were aspirated to  $500~\mu\text{L}$ .  $100~\mu\text{L}$  wormless supernatant from this solution was transferred into a well of a 96 well plate (CELLSTAR® black polystyrene 96-well plate with micro-clear flat bottom, Greiner Bio-one, Austria).  $3\times100~\mu\text{L}$  containing 400 worms each were transferred as triplicate into a 96 well plate. The remaining  $100~\mu\text{L}$  worm suspension was shock frosted in liquid nitrogen and stored at -80~°C for protein measurement, which was determined by BCA analysis (bicinchoninic acid assay-kit (Thermo Scientific)). Bottom read fluorescence measurements of worm-loaded cavities were done in a Tecan Infinite® M Plex Reader ();  $\lambda_{ex}=415~\text{nm}$ ;  $\lambda_{em}=660~\text{nm}$  conducted for wavelengths of 415 nm for excitation and 660 nm for emission for  $p\text{-H}_8\text{-}TBPPA$  or 415 nm and 650 nm for  $p\text{-H}_8\text{-}TBPPA$  using a Tecan microplate reader (Tecan,

Switzerland). The fluorescence intensity of the supernatant was subtracted from the sample intensity for the evaluation.

#### Statistical analysis

Statistical significance of experimental results was calculated by GraphPad prism software version 8.02 (GraphPad Software Inc., CA, USA) using the tests indicated in the respective figure legends.

# X-ray crystallography

Single-crystal X-ray diffraction data, pre-unit cell determinations, for p-H<sub>8</sub>-TBPPA and p-Me<sub>8</sub>-TBPPE were performed with the program suite CrysAlisPro [CrysAlisPro (version 1.171.40.39a), Rigaku Oxford Diffraction (2018)]. The structure was solved using SHELXT and refined by full-matrix least-squares methods on F2 with SHELXL61,62. Hydrogen atoms bonded to carbon were positioned geometrically and refined using the riding model. Crystallographic parameters are summarized in Supplementary Table S1. In the structure of p-H<sub>8</sub>-TBPPA, SQUEEZE was employed to remove diffuse electron density in the porous regions that could not be modeled as discrete solvent molecules<sup>63</sup>. A solvent-accessible volume (SAV) of 7466 Å<sup>3</sup> containing 2061 electrons was identified per unit cell. Since a mixture of DMF and MeOH was present, it was not possible to accurately determine the proportion of each solvent; therefore, no solvent molecules were included in the final chemical formula. In the asymmetric unit of p-Me<sub>8</sub>-TBPPE, both chloroform molecules exhibit disorder. The disorder components were refined with occupancy ratios of 0.67/0.33 and 0.61/0.39, respectively. In the crystal structure of the metal-free porphyrin compound (p-Me<sub>8</sub>-TBPPE), no central metal atom was expected. However, during the structure refinement, a residual electron density peak of 6.18 eÅ-3 was observed at the center of the porphyrin core. This observation suggests the possible partial incorporation of a heavy atom, most likely palladium (Pd), into the porphyrin cavity in the ester form (Supplementary Fig. S7). Crystal data and structure refinement can be found in Supplementary Table S1. The overall chemical formula of p-Me<sub>8</sub>-TBPPE was determined to be C<sub>84</sub>H<sub>72</sub>Cl<sub>24</sub>N<sub>4</sub>O<sub>12</sub>P<sub>4</sub>Pd<sub>0.07</sub>. Additional crystallographic data with CCDC reference numbers 2447121 (p-H<sub>8</sub>-TBPPA) and 2447122 (p-Me<sub>8</sub>-TBPPE) have been deposited within the Cambridge Crystallographic Data Center via www.ccdc.cam.ac.uk/deposit.

## **Data availability**

Supporting Information is available for crystal structure refinement, synthesis and characterization, details of cell culture experiments and fluorescence studies. [CCDC 2447121 and 2447121 contain the supplementary crystallographic data for this paper. These data can be obtained free of charge from The Cambridge Crystallographic Data Centre via www.ccdc. cam.ac.uk/data\_request/cif.]

Received: 14 May 2025; Accepted: 24 September 2025; Published online: 21 October 2025

#### References

- Lutsenko, S. Human copper homeostasis: a network of interconnected pathways. Curr. Opin. Chem. Biol. 14, 211–217 (2010).
- Gaggelli, E., Kozlowski, H., Valensin, D. & Valensin, G. Copper Homeostasis and Neurodegenerative Disorders (Alzheimer's, Prion, and Parkinson's Diseases and Amyotrophic Lateral Sclerosis). *Chem. Rev.* 106, 1995–2044 (2006).
- Maares, M. et al. A fluorometric assay to determine labile copper(II) ions in serum. Sci. Rep. 13, 12807 (2023).
- 4. Weishaupt, A. K. et al. Dysfunction in atox-1 and ceruloplasmin alters labile Cu levels and consequently Cu homeostasis in C. elegans. *Front Mol. Biosci.* **11**, 1354627 (2024).
- 5. Helmann, J. D. Metals in Motion: Understanding Labile Metal Pools in Bacteria. *Biochemistry* **64**, 329–345 (2025).

- Grover, K., Koblova, A., Pezacki, A. T., Chang, C. J. & New, E. J. Small-Molecule Fluorescent Probes for Binding- and Activity-Based Sensing of Redox-Active Biological Metals. *Chem. Rev.* 124, 5846–5929 (2024).
- Zorlu, Y. et al. Fluorescent Arylphosphonic Acids: Synergic Interactions between Bone and the Fluorescent Core. Chemistry 26, 11129–11134 (2020).
- Keil, C. et al. Arylphosphonate-Tethered Porphyrins: Fluorescence Silencing Speaks a Metal Language in Living Enterocytes\*\*. ChemBioChem 22, 1925–1931 (2021).
- Walkup, G. K., Burdette, S. C., Lippard, S. J. & Tsien, R. Y. A New Cell-Permeable Fluorescent Probe for Zn<sup>2+</sup>. J. Am. Chem. Soc. 122, 5644–5645 (2000).
- Kursunlu, A. N. Porphyrin–Bodipy combination: synthesis, characterization and antenna effect. RSC Adv. 4, 47690–47696 (2014).
- Kursunlu, A. N. & Güler, E. Facile assembly of Bodipy-based metal ion sensor using click chemistry. Supramolecular Chem. 25, 512–521 (2013)
- Motekaitis, R. J., Murase, I. & Martell, A. E. Equilibriums of ethylenediamine-N,N,N',N'-tetrakis(methylenephosphonic) acid with copper(II), nickel(II), cobalt(II), zinc(II), magnesium(II), calcium(II), and iron(III) ions in aqueous solution. *Inorg. Chem.* 15, 2303–2306 (1976).
- 13. Linder, M. C. & Hazegh-Azam, M. Copper biochemistry and molecular biology. *Am. J. Clin. Nutr.* **63**, 797S–811S (1996).
- Chen, L., Min, J. & Wang, F. Copper homeostasis and cuproptosis in health and disease. Signal Transduct. Target. Ther. 7, 378 (2022).
- Tholen, P. et al. Tuning Structural and Optical Properties of Porphyrinbased Hydrogen-Bonded Organic Frameworks by Metal Insertion. Small 18, 2204578 (2022).
- Tholen, P. et al. Semiconductive microporous hydrogen-bonded organophosphonic acid frameworks. Nat. Commun. 11, 3180 (2020).
- Lin, R.-B. et al. Multifunctional porous hydrogen-bonded organic framework materials. Chem. Soc. Rev. 48, 1362–1389 (2019).
- Vicent-Morales, M. et al. Semiconductor Porous Hydrogen-Bonded Organic Frameworks Based on Tetrathiafulvalene Derivatives. *J. Am. Chem. Soc.* 144, 9074–9082 (2022).
- 19. Wang, B., Lin, R. B., Zhang, Z., Xiang, S. & Chen, B. Hydrogen-Bonded Organic Frameworks as a Tunable Platform for Functional Materials. *J. Am. Chem. Soc.* **142**, 14399 (2020).
- Wang, B. et al. Microporous Hydrogen-Bonded Organic Framework for Highly Efficient Turn-Up Fluorescent Sensing of Aniline. *J. Am. Chem. Soc.* 142, 12478 (2020).
- He, X.-T. et al. Atomically Thin Nanoribbons by Exfoliation of Hydrogen-Bonded Organic Frameworks for Drug Delivery. ACS Appl. Nano Mater. 2, 2437–2445 (2019).
- Yin, Q. et al. An Ultra-Robust and Crystalline Redeemable Hydrogen-Bonded Organic Framework for Synergistic Chemo-Photodynamic Therapy. *Angew. Chem., Int. Ed.* 57, 7691 (2018).
- Hu, F. et al. An Ultrastable and Easily Regenerated Hydrogen-Bonded Organic Molecular Framework with Permanent Porosity. *Angew. Chem. Int. Ed.* 56, 2101–2104 (2017).
- 24. Li, P., Ryder, M. R. & Stoddart, J. F. Hydrogen-Bonded Organic Frameworks: A Rising Class of Porous Molecular Materials. *Acc. Mater. Res.* **1**, 77–87 (2020).
- Karmakar, A. et al. Hydrogen-Bonded Organic Frameworks (HOFs): A New Class of Porous Crystalline Proton-Conducting Materials. Angew. Chem. Int. Ed. 55, 10667–10671 (2016).
- Karmakar, A. et al. Hydrogen-Bonded Organic Frameworks: Design, Structures and Potential Applications. *Angew. Chem., Int. Ed.* 55, 10667 (2016).
- Schütrumpf, A., Duthie, A., Lork, E., Yücesan, G. & Beckmann, J. Synthesis of Some Di- and Tetraphosphonic Acids by Suzuki Cross-Coupling. Z. f.ür. anorganische und Allg. Chem. 644, 1134–1142 (2018).

- 28. Maares, M. et al. Alkali Phosphonate Metal–Organic Frameworks. *Chem. Eur. J.* **25**, 11214 (2019).
- Deniaud, D. et al. Shape selectivity for alkane hydroxylation with a new class of phosphonate-based heterogenised manganese porphyrins. N. J. Chem. 22, 901–905 (1998).
- Jeffrey, G. A. An introduction to hydrogen bonding. (Oxford University Press, 1997).
- Düren, T., Millange, F., Férey, G., Walton, K. S. & Snurr, R. Q. Calculating Geometric Surface Areas as a Characterization Tool for Metal-Organic Frameworks. J. Phys. Chem. C. 111, 15350 (2007).
- Talu, O. & Myers, A. L. Molecular simulation of adsorption: Gibbs dividing surface and comparison with experiment. AIChE J. 47, 1160–1168 (2001).
- Sarkisov, L., Bueno-Perez, R., Sutharson, M. & Fairen-Jimenez, D. Materials Informatics with PoreBlazer v4.0 and the CSD MOF Database. Chem. Mater. 32, 9849–9867 (2020).
- Gouterman, M. Study of the Effects of Substitution on the Absorption Spectra of Porphin. J. Chem. Phys. 30, 1139–1161 (2004).
- Gouterman, M. Spectra of porphyrins. J. Mol. Spectrosc. 6, 138–163 (1961).
- Jeong, D., Kang, D. -g, Joo, T. & Kim, S. K. Femtosecond-Resolved Excited State Relaxation Dynamics of Copper (II) Tetraphenylporphyrin (CuTPP) After Soret Band Excitation. Sci. Rep. 7, 16865 (2017).
- Kilian, K., Pęgier, M. & Pyrzyńska, K. The fast method of Cu-porphyrin complex synthesis for potential use in positron emission tomography imaging. Spectrochimica Acta Part A: Mol. Biomolecular Spectrosc. 159, 123–127 (2016).
- Quiroz-Segoviano, R. I. Y. et al. On Tuning the Fluorescence Emission of Porphyrin Free Bases Bonded to the Pore Walls of Organo-Modified Silica. *Molecules* 19, 2261–2285 (2014).
- Uttamlal, M. & Sheila Holmes-Smith, A. The excitation wavelength dependent fluorescence of porphyrins. *Chem. Phys. Lett.* 454, 223–228 (2008).
- Zakavi, S. & Hoseini, S. The absorption and fluorescence emission spectra of meso-tetra(aryl)porphyrin dications with weak and strong carboxylic acids: a comparative study. RSC Adv. 5, 106774–106786 (2015).
- Schmitt, F.-J. et al. eGFP-pHsens as a highly sensitive fluorophore for cellular pH determination by fluorescence lifetime imaging microscopy (FLIM). *Biochimica et. Biophysica Acta ((BBA)) - Bioenerg.* 1837, 1581–1593 (2014).
- Schmitt, F. J. et al. Time resolved temperature switchable excitation energy transfer processes between CdSe/ZnS nanocrystals and phycobiliprotein antenna from Acaryochloris marina. *Photonics Nanostruct. - Fundamentals Appl.* 9, 190–195 (2011).
- Au, C. et al. SMF-1, SMF-2 and SMF-3 DMT1 Orthologues Regulate and Are Regulated Differentially by Manganese Levels in C. elegans. PLOS ONE 4, e7792 (2009).
- 44. Märk, J. et al. Photoacoustic imaging of fluorophores using pumpprobe excitation. *Biomed. Opt. Express* **6**, 2522–2535 (2015).
- Vitali, M. et al. A Single-Photon Avalanche Camera for Fluorescence Lifetime Imaging Microscopy and Correlation Spectroscopy. *IEEE J. Sel. Top. Quantum Electron.* 20, 344–353 (2014).
- 46. Tejwani, V. et al. Investigation of the NADH/NAD+ ratio in Ralstonia eutropha using the fluorescence reporter protein Peredox. *Biochimica et. Biophysica Acta ((BBA)) Bioenerg.* **1858**, 86–94 (2017).
- Zorlu, Y. et al. Electrically Conductive Photoluminescent Porphyrin Phosphonate Metal–Organic Frameworks. Adv. Optical Mater. 10, 2200213 (2022).
- Chillon, T. S. et al. Combined copper and zinc deficiency is associated with reduced SARS-CoV-2 immunization response to BNT162b2 vaccination. Heliyon 9, e20919 (2023).
- Kirsipuu, T. et al. Copper(II)-binding equilibria in human blood. Sci. Rep. 10, 5686 (2020).

- Núñez, M. T., Tapia, V., Toyokuni, S. & Okada, S. Iron-induced oxidative damage in colon carcinoma (caco-2) cells. *Free Radic. Res.* 34, 57–68 (2001).
- Baesler, J. et al. Nutritive Manganese and Zinc Overdosing in Aging C. elegans Result in a Metallothionein-Mediated Alteration in Metal Homeostasis. Mol. Nutr. Food Res. 65, 2001176 (2021).
- Gremme, A. et al. Is Ferric the Same as Ferrous? Effect of Nutritionally Relevant Iron Species in C. elegans: Bioavailability, Iron Homeostasis, Oxidative Stress, and Cell Death. J. Agric Food Chem. 73, 3714–3723 (2025).
- Chun, H. et al. The Intestinal Copper Exporter CUA-1 Is Required for Systemic Copper Homeostasis in Caenorhabditis elegans. *J. Biol. Chem.* 292, 1–14 (2017).
- Yuan, S., Sharma, A. K., Richart, A., Lee, J. & Kim, B. E. CHCA-1 is a copper-regulated CTR1 homolog required for normal development, copper accumulation, and copper-sensing behavior in Caenorhabditis elegans. *J. Biol. Chem.* 293, 10911–10925 (2018).
- Alker, W., Schwerdtle, T., Schomburg, L. & Haase, H. A Zinpyr-1based Fluorimetric Microassay for Free Zinc in Human Serum. *Int. J. Mol. Sci.* 20, (2019).
- Schmitt, F. J. et al. Effect of Molecular Dynamics and Internal Water Contact on the Photophysical Properties of Red pH-Sensitive Proteins. *Biochemistry* 63, 82–93 (2024).
- Pinto, M. Enterocyte-like differentiation and polarization of the human colon carcinoma cell line Caco-2 in culture. *Biol. Cell* 47, 323–330 (1983).
- Ferraretto, A. et al. Morphofunctional properties of a differentiated Caco2/HT-29 co-culture as an in vitro model of human intestinal epithelium. *Biosci. Rep.* 38 https://doi.org/10.1042/bsr20171497 (2018).
- Maares, M., Duman, A., Keil, C., Schwerdtle, T. & Haase, H. The impact of apical and basolateral albumin on intestinal zinc resorption in the Caco-2/HT-29-MTX co-culture model. *Metallomics* 10, 979–991 (2018).
- Nass, R. & Hamza, I. The nematode C. elegans as an animal model to explore toxicology in vivo: solid and axenic growth culture conditions and compound exposure parameters. *Curr. Protoc. Toxicol.* Chapter 1, Unit1.9 https://doi.org/10.1002/0471140856.tx0109s31 (2007).
- Sheldrick, G. M. Crystal Structure Refinement with SHELXL. Acta Crystallogr., Sect. C: Struct. Chem. 71, 3 (2015).
- Sheldrick, G. M. SHELXT-Integrated Space-Group and Crystal-Structure Determination. *Acta Crystallogr.*, Sect. A: Found. Adv. 71, 3 (2015).
- 63. Spek, A. Structure validation in chemical crystallography. *Acta Crystallogr. Sect. D.* **65**, 148–155 (2009).

# **Acknowledgements**

G.Y. would like to thank DFG for research grants YU 267/2-1 and YU 267/ 9-1

## **Author contributions**

P.T. synthesized the compounds, obtained the crystals, obtained the crystal structures, performed the fluorescence experiments with different metal ions, contributed to the introduction part and wrote the synthesis part. A.K.W. performed the experiments related to *C. elegans* studies. F.J.S. performed the fluorescence lifetime experiments and wrote the corresponding section. T.M and J.F. performed the NMR experiments and interpreted the NMR data. T.V.M.N. contributed to the fluorescence experiments and performed the cytotoxicity analysis. C.K. supervised the fluorescence measurements, organized collaborations, contributed, critically read and revised the manuscript. M.M. supervised the the cell experiments and toxicity analysis and contributed to the related text. L.S. performed the ceruloplasmin related work and wrote the related text. H.H. critically read and revised the manuscript. Y.Z. refined the crystal structures

and generated the crystallographic figures. J.B. supervised the synthesis of precursors for the Suzuki Coupling at University of Bremen, critically read and revised the manuscript. J.B. supervised the *C. elegans* studies wrote the corresponding sections in the introduction and experimental section, critically read and revised the manuscript. G.Y. created the hypothesis, supervised the work of P.T., contributed to the introduction and conclusion, organized collaborations, critically revised and edited the manuscript.

# **Funding**

Open Access funding enabled and organized by Projekt DEAL.

# **Competing interests**

Gündoğ Yücesan and Hajo Haase have two patent applications. Yücesan, G. & Haase, H. Fluorescent probes for detection of calcifications. US Patent Application 17/802,759 (2023). Yücesan, G. & Haase, H. Fluorescent probes for quantification of free copper. US Patent Application 18/026,773 (2024). The other authors declare no competing interest.

# **Additional information**

**Supplementary information** The online version contains supplementary material available at https://doi.org/10.1038/s43246-025-00975-0.

**Correspondence** and requests for materials should be addressed to Claudia Keil or Gündog Yücesan.

**Peer review information** *Communications Materials* thanks C. Immanuel David and the other, anonymous, reviewer(s) for their contribution to the peer review of this work.

**Reprints and permissions information** is available at http://www.nature.com/reprints

**Publisher's note** Springer Nature remains neutral with regard to jurisdictional claims in published maps and institutional affiliations.

Open Access This article is licensed under a Creative Commons Attribution 4.0 International License, which permits use, sharing, adaptation, distribution and reproduction in any medium or format, as long as you give appropriate credit to the original author(s) and the source, provide a link to the Creative Commons licence, and indicate if changes were made. The images or other third party material in this article are included in the article's Creative Commons licence, unless indicated otherwise in a credit line to the material. If material is not included in the article's Creative Commons licence and your intended use is not permitted by statutory regulation or exceeds the permitted use, you will need to obtain permission directly from the copyright holder. To view a copy of this licence, visit http://creativecommons.org/licenses/by/4.0/.

© The Author(s) 2025